Characterization of the Martian Convective Boundary Layer

GERMÁN MARTÍNEZ, FRANCISCO VALERO, AND LUIS VÁZQUEZ

Universidad Complutense de Madrid, Madrid, Spain

(Manuscript received 6 November 2008, in final form 16 January 2009)

ABSTRACT

The authors have carried out an extensive characterization of the Martian mixed layer formed under convective conditions. The values of the mixed layer height, convective velocity scale, convective temperature scale, mean temperature standard deviation, mean horizontal and vertical velocity standard deviations, and mean turbulent viscous dissipation rate have been obtained during the strongest convective hours for the mixed layer. In addition, the existing database of the surface layer has been improved by recalculating some parameters (e.g., Monin–Obukhov length, friction velocity, or scale temperature) that had already been obtained in previous papers by other means and also by calculating new ones, such as the standard deviation of the vertical wind speed velocity, the turbulent viscous dissipation rate, and eddy transfer coefficients for momentum and heat. The Earth counterparts of all these magnitudes are also shown. In this paper, a comprehensive database concerning the whole convective planetary boundary layer on Mars is displayed, and a detailed terrestrial comparison is established.

The inputs of this work are hourly in situ temperature, hourly in situ horizontal wind speed, and hourly simulated ground temperature for specific selected Sols of the Viking and Pathfinder landers. These data correspond to typical low and midlatitude northern summertime conditions, with weak prevailing winds. To handle this set of data, surface layer and mixed layer similarity theory have been used at the strongest convective hours. In addition, the inclusion of a parameterization of a molecular sublayer and prescribed values of the surface roughness has been considered.

1. Introduction

The mixed layer is one of the three layers into which the convective boundary layer can be divided, with the surface layer and the entrainment zone lying respectively beneath and above it. It is characterized by an intense vertical mixing that tends to leave variables such as potential temperature and humidity nearly constant with height, even wind speed and direction (Stull 1988). On Earth, it typically encompasses 40%–70% of the convective boundary layer height. The Martian planetary boundary layer (MPBL), and specifically the Martian mixed layer (MML), is one of the least-known parts of the Martian atmosphere. This is so, among other minor aspects, because of (i) the lack of in situ data covering the MML, (ii) some specific Martian features such as the atmospheric dust load, and (iii) its own intrinsic turbulent nature. Nevertheless, its understanding becomes quite important for several reasons. First, it is the place through which current and future robotic and manned missions will be sent. Therefore, at least partial knowledge of its dynamical and thermal behavior is needed for the design of both the spacecrafts and sensors. In addition, small-scale processes ''belonging'' to the MML have an impact on larger-scale processes, and vice versa. As a consequence, general circulation models and mesoscale models need to incorporate MML effects to simulate more accurately the real atmospheric behavior.

Up to now, there have been three kinds of papers referring to the MPBL literature. The first kind concerns analytical 1D (Gierasch and Goody 1968; Blumsack et al. 1973; Magalhaes and Gierasch 1982; Ye et al. 1990; Savijärvi 1991; Haberle et al. 1993; Savijärvi 1995, 1999; Savijärvi et al. 2004; Määttänen and Savijärvi 2004), 2D (Savijärvi and Siili 1993; Siili et al. 1997; Odaka 2001), and 3D models (Rafkin et al. 2001; Toigo and Richardson 2002). These papers (1D, 2D, and 3D models) mostly show three kinds of results: (i) vertical profiles of temperature, wind speed, heating rates (radiative and turbulent), and kinematic heat flux at

Corresponding author address: Germán Martínez, Dept. de Ciencias de la Atmósfera y Astrofísica II, Facultad de Física, Universidad Complutense de Madrid, Madrid 28040, Spain.
E-mail: mmgerman@fis.ucm.es

DOI: 10.1175/2009JAS3007.1

© 2009 American Meteorological Society

Unauthenticated | Downloaded 12/10/24 11:25 AM UTC

specific hours; (ii) diurnal evolutions of magnitudes that have been measured in situ to test the model (i.e., temperature and wind speed near the ground); and (iii) the energy balance at the ground. However, no MML turbulent parameters (turbulent statistics, fundamental mixed layer similarity scales, dissipation rate across the MML, etc.) are shown through them.

The second kind of papers refers to surface layer similarity models, which need simulated ground temperature and in situ wind and temperature measurements at the first meters (Sutton et al. 1978; Tillman et al. 1994; Larsen et al. 2002; Martinez et al. 2009). They all use surface layer similarity theory; therefore, only Martian surface layer (MSL) parameters are calculated, except for the mixed layer height.

Large-eddy simulation (LES) models form the third kind of papers (Rafkin et al. 2001; Michaels and Rafkin 2004; Toigo et al. 2003; Sorbjan 2007a,b). In principle they are supposed to perform with the highest accuracy throughout the MML, although they require expensive computational time. Examining them in detail, Rafkin et al. (2001) show vertical wind speed variance $\sigma_w^2(z,t)$ and turbulent kinetic energy $e(z, t)$ as functions of height z and time t, albeit for a generic run [see Rafkin et al. (2001, p. 246) for details of the generic run]. Michaels and Rafkin (2004) comment on the qualitative behavior of $\sigma_w^2(z,t)$ and $e(z,t)$ for Pathfinder conditions, but none of the MML magnitudes presented here are displayed. On the other hand, Sorbjan (2007a,b) does show turbulent statistics and fundamental mixed layer similarity scales (mixed layer height, convective velocity scale, and convective temperature scale), although for a generic run (see Table 2 of Sorbjan 2007a and Table 1 of Sorbjan 2007b) and in a dimensionless form.

Noticing the current state of the art, we have carried out specific research about the MML by calculating the characteristic parameters of the mixed layer: mixed layer height z_i, convective velocity scale w_*, convective temperature scale θ_*, mean horizontal $\langle\sigma_u\rangle$ and vertical $\langle\sigma_w\rangle$ velocity standard deviations, mean temperature standard deviation $\langle\sigma_\theta\rangle$, and mean turbulent viscous dissipation rate $\langle\epsilon\rangle$, where the angled brackets denote averaging over the whole mixed layer. Our second goal has been to review and complete the existing Martian surface layer database. In reviewing it, we have recalculated some MSL parameters, namely the Monin–Obukhov length L, friction velocity u_*, and temperature scale T_*. These magnitudes had already been estimated by other means in previous papers; see Martinez et al. (2009) for a complete MSL review. In completing the MSL database, we have derived—for the first time from in situ data and similarity relationships—new MSL magnitudes, such as the turbulent viscous dissipation rate ϵ^z, standard deviation of vertical wind speed σ_w^z, and eddy transfer coefficients for heat k_h^z and momentum k_m^z, where the superscript z denotes the height at which they have been calculated [1.3 m for the Pathfinder (PF) and 1.6 m for the Viking (VK) Landers]. In short, this paper displays an extensive database covering the whole MPBL, from the MSL up to the MML. In addition, references and typical values for all the counterpart terrestrial magnitudes are given to allow a direct comparison with the terrestrial boundary layer. Definitions and conceptual meanings of each of the magnitudes calculated above are given in appendix A.

Even at present, the Viking and Pathfinder missions still provide the most suitable in situ data for performing micrometeorological research. Static simultaneous measurements of wind speed and atmospheric temperature monitored with a high sample rate and during times on the order of 1 h without interruptions, have been taken by only these two missions. Mars Exploration Rover and Phoenix data are also useful, although they do not satisfy the restrictions above. This is why we have calculated all these magnitudes at VK and PF sites. To do so, we have used (i) in situ temperature and horizontal wind speed data, (ii) simulated ground temperature, and (iii) surface layer and mixed layer similarity theory, together with a parameterized molecular sublayer and prescribed values of the surface roughness.

A warning about the nature of these data must be stated at this point. As will be discussed in the next section, the observations of this work belong to typical low midlatitude northern summertime Sols. Under such conditions, the mean wind is very weak, and consequently the mixed layer formed is mainly convectively driven. Therefore, our results are generic for such conditions.

Section 2 deals with the data that form the input of this work. There we explain why they are the most accurate ones representing VK and PF sites. In section 3, we analyze the methodology used to derive the results of this paper; the results themselves are presented in section 4. This, in turn, is divided into three subsections, discussing the fundamental similarity scales, the turbulent statistics, and the turbulent viscous dissipation rate, together with the eddy diffusivity coefficients for heat and momentum. In each of them, the results are shown both for the MML and for the MSL. Section 5 also contains three subsections. In the first one, we compare the MML and MSL values. A description of the sensitivity of the results to the inclusion of a molecular sublayer, to the surface roughness, and finally to the created ground temperature scenarios is shown and explained in next subsection. The third subsection shows terrestrial counterparts for all our derived

Unauthenticated | Downloaded 12/10/24 11:25 AM UTC

TABLE 1. Measurement errors at the Viking locations.

	Sols 1–44		Sols > 44	
	T	U	*T*	*U*
VL-1	±1.5 K	±10%	Good data	Degraded
VL-2	±2 K	±10%	Problems	±10%

magnitudes, including a comment about the existing analogies and differences between the two planets. The paper ends with section 6, where we offer a brief summary of the paper and we present the main conclusions.

2. Data

Three sets of data form the input for this analysis: in situ temperature and in situ horizontal wind speed (at 1.3 m for PF and 1.6 m for VK), together with hourly simulated ground temperature. They all belong to some selected Sols of VK and PF missions. For detailed information on both missions, see Hess et al. (1977) and Schofield et al. (1997).

Because the reliability of this work strongly depends on the quality of the input, we will detail why and how we have selected them. Sols 27, 28, and 35 of Viking Lander 1 (VL1), Sols 20 and 25 of Viking Lander 2 (VL2), and Sol 25 of PF were chosen. They correspond to a solar longitude of about 110°, 127°, and 155° for the VL1, VL2, and PF Sols, respectively. In choosing the VK Sols, the following were taken into account: lander interferences, sensor sampling rates, the accuracy of the sensors, the time of the year, and the amount of atmospheric dust. Data from the above VK Sols fulfill the most optimal conditions; that is, prevailing wind direction involved the least lander interferences. On the other hand, the wind speed and temperature sampling rate during the strongest convective hours were the highest possible (implying more accurate means and variances). In addition, the accuracy of the sensors was at its highest level (see Table 1). With regards to the time of the year, it was northern summertime. Through this season, the MPBL is typically convectively driven, since baroclinic disturbances are not present. As a result, mixed-layer similarity theory can still be applied. Finally, the amount of atmospheric dust was at its minimum, which could also hinder the application of similarity theory. In contrast, the reason for selecting PF Sol 25 is easier to describe: this is the only Sol for which temperature and horizontal velocity measurements are available to us during an entire Sol. In addition, the measurements correspond to typical summertime conditions, characteristics needed in this work.

TABLE 2. 1D model parameters used to create the MPS for VL1 Sols 27, 28, and 35, VL2 Sols 20 and 25, and PF Sol 25; $T(1)$ is the initial ground temperature, G_A refers to the initial vertical temperature lapse rate, U_{G0} is the geostrophic wind speed, z_0 is the surface roughness, G_i is the thermal inertia, τ is the dust optical depth, α is the surface albedo, and SE is the surface emissivity.

	$T(1)$ (K)	G_A (K km^{-1})	U_{G0} (m s^{-1})	z_0 (m)	G_i (S.I)	τ	α	SE
VL-1	215	2	10	0.01	269	0.4	0.22	0.95
VL-2	215	2	0	0.01	234	0.5	0.23	0.90
PF	225	2	10	0.01	387	0.2	0.19	0.90

Specifically, for the VK Sols, mean hourly values of horizontal wind speed and temperature are straightforwardly shown in the National Aeronautics and Space Administration (NASA) Planetary Data System (PDS), as are the sensor sampling rates (number of measurements each hour). On the other hand, only 0.25-Hz temperature measurements are found in the PDS corresponding to PF Sol 25. Horizontal wind speed measurements, also monitored at 0.25 Hz during the entire Sol, have been kindly provided by Dr. Jim Murphy because the wind sensor experienced problems. Thus, we have simply hourly averaged these temperature and horizontal wind speed data to obtain the hourly outputs in the PF case. As a result, in Figs. 1 and 2 we can see the horizontal wind speed and temperature data corresponding to the Sols under study.

Special care has been taken when considering the ground temperature T_g because it is the only non–in situ input. We have simulated T_g for all the Sols under study (see Fig. 3) using a modified version (see Table 2) of the 1D model Savijärvi et al. (2004). The procedure for deriving the ground temperature for the selected Sols is a tricky issue, and appendix B clarifies how this quantity was obtained.

3. Methodology

We now show the methodology employed to obtain our results. The method of deriving L, $u*$, $T*$, ϵ^z, k_m^z, and k_h^z from our input is detailed in Martinez et al. (2009). Turning to the MSL turbulent statistics, we have calculated σ_w^z by using the surface layer similarity relationship

$$\frac{\sigma_w^z}{u*} = 1.3[1 + 3(-z/L)]^{1/3} \quad (1)$$

given by Panofsky et al. (1977). On the other hand, the horizontal velocity standard deviation σ_u^z and temperature standard deviation σ_T^z have been directly inferred from the in situ temperature and horizontal velocity measurements from the VK and PF missions.

Unauthenticated | Downloaded 12/10/24 11:25 AM UTC

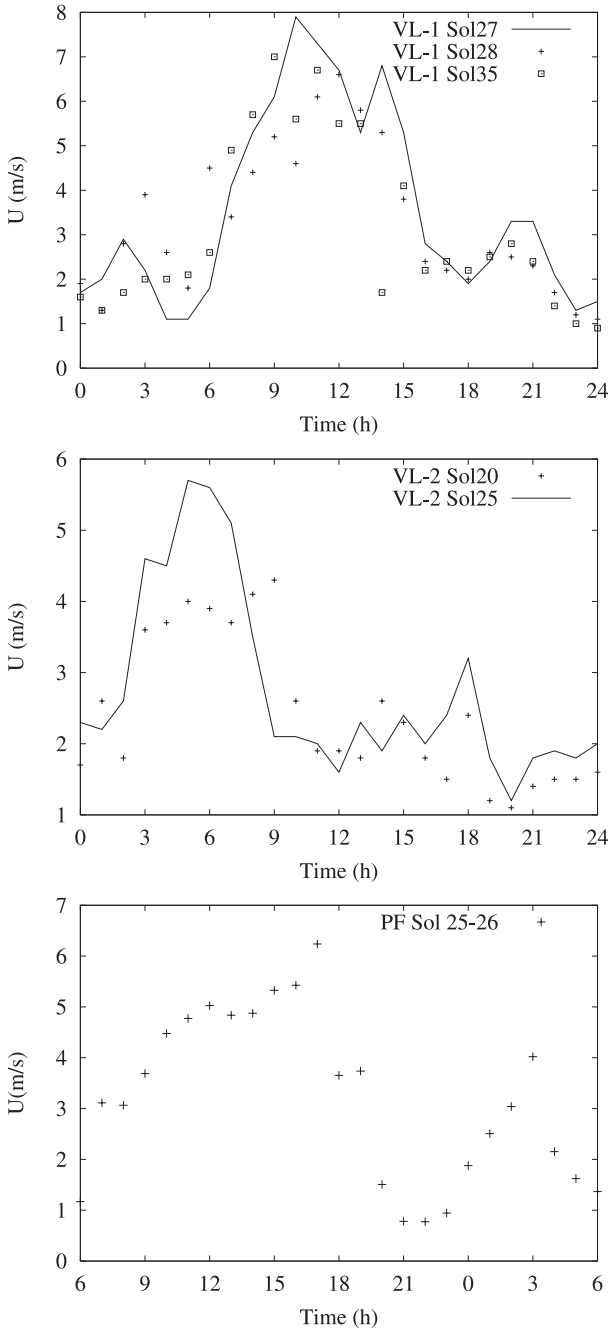

FIG. 1. In situ horizontal wind speed at 1.6 m for VL1 and VL2 and 1.3 m for the PF during the selected Sols.

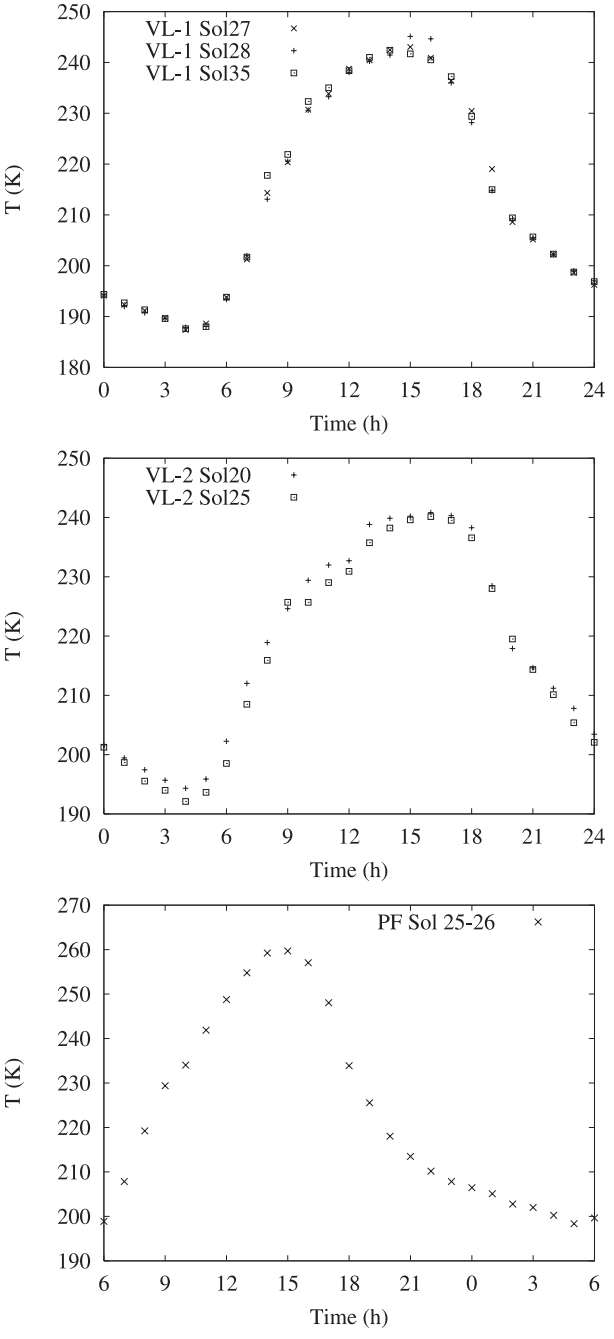

FIG. 2. As in Fig. 1, but for in situ temperature.

Once the MSL parameters have been obtained, the relation that enables us to link the MSL to the MML is

$$\frac{\sigma_u^z}{u_*} = [12 + 0.5(z_i/|L|)]^{1/3}, \tag{2}$$

given by Panofsky et al. (1977). Here it has been supposed that the horizontal velocity standard deviation scales with the convective velocity scale w_* because the horizontal component of the convective eddies is expected to extend down to the surface. Equation (2) allows us to calculate the mixed layer height z_i and hence the convective velocity, defined as $w_* = (-u_* T_* z_i g/T_g)^{1/3}$, and also the convective temperature scale, defined as $\theta_* = -u_* T_*/w_*$.

Unauthenticated | Downloaded 12/10/24 11:25 AM UTC

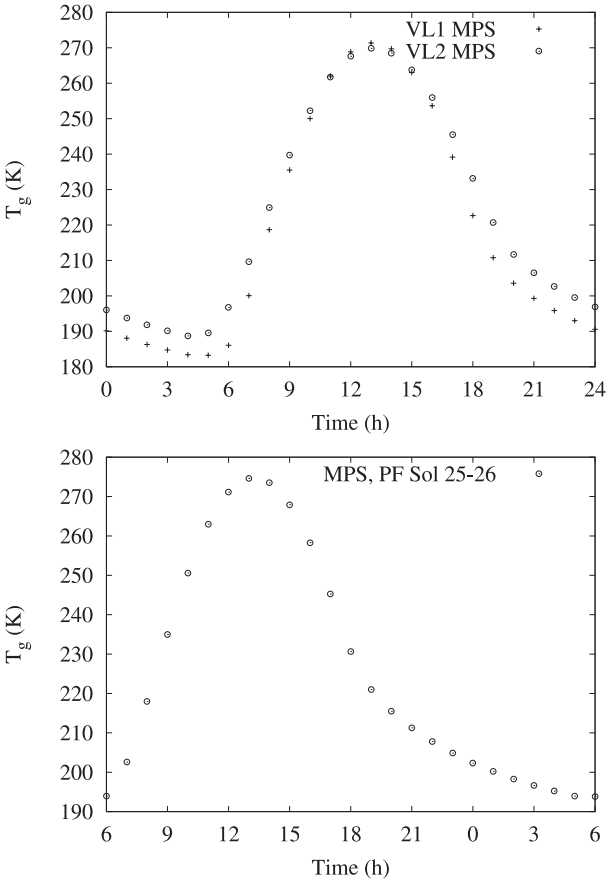

FIG. 3. Most probable ground temperature scenario for the VL1 Sol 27, VL2 Sol 20, and PF Sol 25. The most probable scenarios corresponding to the other Sols are very similar to the ones displayed above and therefore are not shown.

At this point we have values for the fundamental mixed layer similarity scales, namely z_i, w_*, and θ_*. Consequently, mixed layer similarity theory (Deardorff 1970) could be applied in principle. However, its applicability on Mars is not as clear as on Earth. Because we have employed this theory to obtain our results, we have created appendix C to explain the reliability of its use in the MML.

During the morning hours, in which convection is the dominant heating mechanism, we have calculated all the mixed layer magnitudes. Thus, $\langle\sigma_w\rangle$, $\langle\sigma_u\rangle$, and $\langle\sigma_\theta\rangle$ have been obtained by integrating along the MML the next mixed layer similarity relations

$$\frac{\sigma_w}{w_*} = (1.8)^{0.5}(1 - 0.8z/z_i)^{1/3}, \tag{3}$$

$$\frac{\sigma_u}{w_*} \simeq \frac{\langle\sigma_u\rangle}{w_*} = 0.6, \quad \text{and} \tag{4}$$

$$\frac{\sigma_\theta}{\theta_*} = (1.8)^{0.5}(z/z_i)^{-1/3}, \tag{5}$$

with Eq. (3) from Lenschow et al. (1980), Eq. (4) from Arya (2001), and Eq. (5) from Kaimal et al. (1976). Finally, the mean turbulent viscous dissipation rate

$$\langle\epsilon\rangle = \frac{0.5w_*^3}{z_i} \tag{6}$$

has been derived from Kaimal et al. (1976). Notice that in this case, the term $2\epsilon z_i/{w_*}^3$ formed by making ϵ nondimensional does not depend on z/z_i, as it happens to σ_u in (4). Thus, in both cases, the mean value across the mixed layer matches the value at each height.

As an alternative procedure, we have calculated $\langle\sigma_w\rangle$ and $\langle\sigma_\theta\rangle$ from MSL parameters

$$\frac{\langle\sigma_w\rangle}{u_*} = 0.8(z_i/|L|)^{1/3} \quad \text{and} \tag{7}$$

$$\frac{\langle\sigma_\theta\rangle}{T_*} = -1.2(z_i/|L|)^{-1/3}, \tag{8}$$

with Eqs. (7) and (8) from Tennekes (1970). The following conditions need to be met to obtain these two last relations: a balance between buoyancy and dissipation across the mixed layer, and a high correlation between temperature and vertical velocity turbulent fluctuations.

4. Results

The results are divided into three different sections, dealing with (i) fundamental similarity scales, (ii) turbulent statistics, and (iii) the turbulent viscous dissipation rate, together with eddy transfer coefficients. In each of the sections, we distinguish between MML magnitudes and their MSL counterparts. Thus, concerning the fundamental similarity scales, z_i, w_*, and θ_* have been determined for the MML and L, u_*, and T_* for the MSL. With regard to the turbulent statistics, $\langle\sigma_u\rangle$, $\langle\sigma_w\rangle$, and $\langle\sigma_\theta\rangle$ have been determined for the MML, as have their MSL counterparts σ_u^z, σ_w^z, and σ_θ^z at the measuring height. Finally, $\langle\epsilon\rangle$ has been determined for the MML and ϵ^z, k_m^z, and k_h^z for the MSL, also at the measuring height.

All the following figures and tables displayed in this section have been calculated under the most probable scenario (MPS) of the ground temperature (see appendix B), after including a parameterized molecular sublayer (Brutsaert 1982), and with the prescribed value of $z_0 = 1$ cm. In addition, although not explicitly shown, we have also calculated all the magnitudes under the three simulated ground temperature scenarios, with and without the inclusion of the molecular sublayer, and for each of the given values of the surface roughness z_0 (0.1, 1,

Unauthenticated | Downloaded 12/10/24 11:25 AM UTC

TABLE 3. Mean values of the fundamental surface layer similarity scales during the convective hours of the three missions. For the VLs, the values shown correspond to the average performed on a composite Sol formed by Sols 27, 28, and 35 for VL1 and Sols 20 and 25 for VL2.

	VL1	VL2	PF
L (m)	−40	−7	−25
u_* (m s^{-1})	0.5	0.25	0.4
T_* (K)	−1.5	−2.5	−1

and 10 cm). This has allowed us to perform sensitivity studies regarding the inclusion of the molecular sublayer (with fixed value of $z_0 = 1$ cm and under the MPS), considering the surface roughness (under the MPS and with the molecular sublayer included), and considering the ground temperature scenario (with fixed value of $z_0 =$ 1 cm and with the inclusion of the molecular sublayer). These sensitivity studies will be shown in section 5.

a. Fundamental similarity scales

1) SURFACE LAYER

The approach followed to derive L, u_*, and T_* can be seen in Martinez et al. (2009), where these magnitudes were calculated for the PF Sol 25. Instead of displaying their diurnal evolutions [something already done by other authors, as in Sutton et al. (1978) and Tillman et al. (1994)], we indicate our obtained mean values in Table 3 , noting that by ''mean values'' we mean their average value during the strongest convective hours.

The Monin–Obukhov length was found to lie between −7 and −40 m. Although not shown, it has determined that Monin–Obukhov length becomes slightly lower without the inclusion of the molecular sublayer, keeping the order of magnitude unchanged. It grows with the surface roughness and, as is expected, $|L^W| < |L^{\mathrm{MPS}}| < |L^C|$ under unstable situations; here, W indicates the warmest scenario and C indicates the coolest (see appendix B for details). However, the absolute difference between L^{MPS} and L calculated under the warmest or coolest scenario is never greater than 4 or 5 m.

For the friction velocity we have obtained values between 0.25 and 0.50 m s^{-1} and have found that it shows virtually no difference whether the molecular sublayer is included or not. It has also been found that the friction velocity increases with the surface roughness, and under unstable conditions its value does not virtually change with the different ground temperature scenarios.

Finally, we have calculated scale temperature values to lie between −1 and −2.5 K. According to our results, it decreases, as we expected, about 35% with the inclusion of the molecular sublayer. It does not show dependence on z_0, and the highest values are to be found for the warmest scenario ($|T_*^W| > |T_*^{\mathrm{MPS}}| > |T_*^C|$), since the difference in temperature between the ground level and 1-m height is the maximum. Differences are quite small, however, around 0.5 K between extreme values.

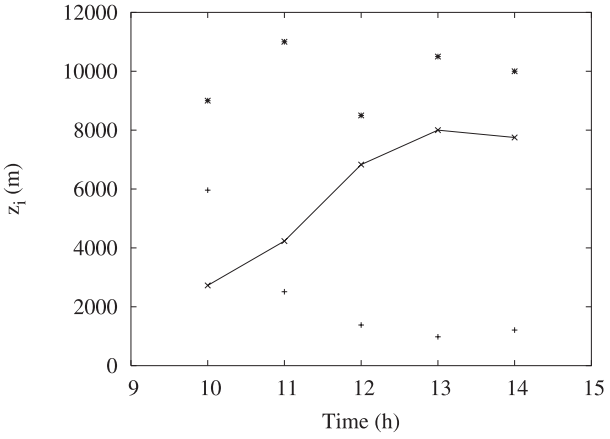

FIG. 4. Mixed layer height during the strongest convective hours for the three missions. For VK, the values shown correspond to the average performed on a composite Sol formed by Sols 27, 28, and 35 for VL1 and Sols 20 and 25 for VL2. The solid line corresponds to the composite Sol of VL1 mission; plus signs indicate the VL2 composite Sol and asterisks indicate the PF Sol.

The dependence of the above magnitudes on the molecular sublayer is expected because in this sublayer only molecular transfer is important for heat, whereas if we consider momentum, then pressure fluctuations—in addition to the molecular transport—are very relevant and accordingly the net effect on the transport of momentum is less noticeable (Zeng and Dickinson 1998). Thus, the main consequence found with the inclusion of the molecular sublayer is a reduction of T_* for a given difference between air temperature and surface skin temperature.

2) MIXED LAYER

We have obtained the mixed layer height z_i from Eq. (2). This relationship satisfies the fact that the ratio σ_u^z/u_* becomes proportional to w_* at large $-z_i/L$ values (convective conditions). Its evolution under strong convection for the three sites is displayed in Fig. 4. It can be noticed that z_i values are around several kilometers in height. These values match other z_i estimations made using different approaches (1D models, LES, or surface layer similarity theories). As an example, Haberle et al.'s (1993) 1D model calculates $z_i \simeq 4$ km at noon for the VL1 summertime. Tillman et al. (1994) estimates $z_i \in (3.5, 9.1)$ km for both VK sites. Concerning LES, for a generic run, Rafkin et al. (2001) calculate $z_i \sim 7$ km, whereas Michaels and Rafkin (2004) obtain $z_i^{\max} \simeq 6$–7 km

Unauthenticated | Downloaded 12/10/24 11:25 AM UTC

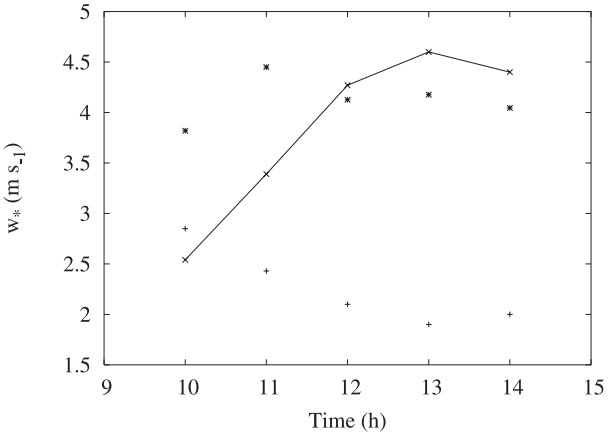

FIG. 5. As in Fig. 4, but for the convective velocity scale.

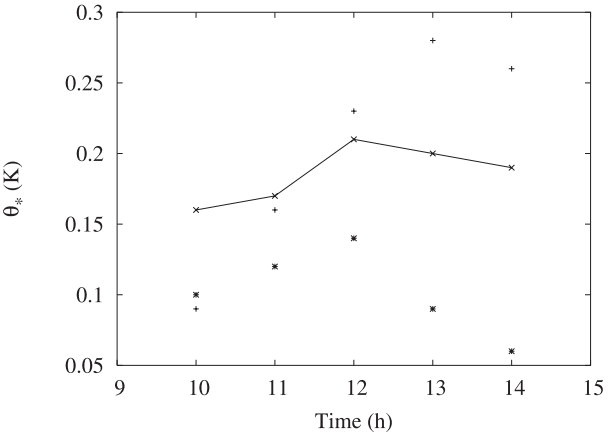

FIG. 6. As in Fig. 4, but for the convective temperature scale.

for the PF site. Turning to the relations of dependence, it has been found that mixed layer height grows with the molecular sublayer, around 20%–30%, because although u_* is insensitive to its inclusion, L does depend on it [see Eq. (2)]. Also, from Eq. (2) it is clear that z_i decreases with z_0 because the u_* surface roughness dependence becomes stronger than L dependence, given that the former is raised to -3. Finally, the facts that during the unstable hours u_* remains unchanged under the three T_g scenarios and that $|L^C| > |L^{\mathrm{MPS}}| > |L^W|$ imply that $z_i^C > z_i^{\mathrm{MPS}} > z_i^W$, being the difference between the coldest or warmest scenario and the most probable scenario not higher than 16%.

The convective velocity scale has been obtained from its definition $w_* = (-u_* T_* z_i g/T_g)^{1/3}$, and its values, which range from 2 to 4.5 m s^{-1}, are shown in Fig. 5. Other Martian w_* estimations, performed for a generic run, can be found in Sorbjan (2007a,b), where values around 3.3 m s^{-1} are determined. Notice that the comparison with these two papers should only be performed near 1000 local time (LT) because the Boussinesq approximation was employed there and therefore Sorbjan's results are restricted to shallow boundary layers, which would correspond to the early hours of the Martian day. This statement is valid for all the following comparisons made between our results and Sorbjan's. The convective velocity scale shows dependence neither on the inclusion of the molecular sublayer nor on the surface roughness or the different T_g scenarios, as could be expected from its definition and the u_*, T_*, and z_i relations of dependence.

The last fundamental mixed layer similarity scale that we have calculated is the convective temperature scale $\theta_* = -T_* u_*/w_*$. Its values for the three Martian sites are displayed in Fig. 6 and lie within the range 0.1 to 0.3 K, similar to the value of 0.3 K obtained in Sorbjan (2007a) for a generic run. It has been found that it decreases with the inclusion of the molecular sublayer via T_* because u_* and w_* show no dependence. Although not physically expected, θ_* grows with the surface roughness a little bit because u_* dependence is not totally counteracted by T_* dependence. The convective temperature scale presents the highest/lowest values under the warmest/coolest scenario, as can be inferred from its definition and the relations of dependence of u_*, w_*, and T_*. In any case, the variation between the extreme values is smaller than 15%.

b. Turbulent statistics

1) SURFACE LAYER

Values of σ_u^z and σ_T^z have been straightforwardly inferred from the in situ temperature and velocity measurements at the VL and PF sites; the mean values for the strongest convective hours can be seen in Table 4. In addition, we have estimated σ_w^z by using Eq. (1), and its results are shown in Fig. 7. Note that σ_w^z is around 4 times lower than σ_u^z, and so vertical turbulence is dominated by horizontal turbulence, mainly because the measuring height was quite close to the ground. Standard deviation values for vertical velocity are slightly higher when calculated without the inclusion of the molecular sublayer because of the dependence that $|L|$ presents on its inclusion. Vertical velocity standard deviation grows

TABLE 4. In situ mean magnitude of the temperature and horizontal wind speed standard deviations during the convective hours of the three missions at around 1.6 m (VK) and 1.3 m (PF). For VK, the values shown correspond to the average performed on a composite Sol formed by Sols 27, 28, and 35 for VL1 site and Sols 20 and 25 for VL2.

	VL1	VL2	PF
σ_u^z (m s^{-1})	2.5	1.3	2.5
σ_T^z (K)	3.0	2.7	3.5

Unauthenticated | Downloaded 12/10/24 11:25 AM UTC

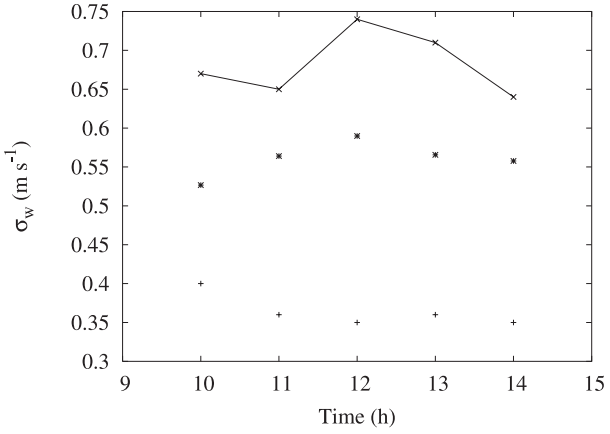

FIG. 7. Vertical wind speed standard deviation during the strongest convective hours for the three missions. The solid line corresponds to the composite Sol of VL1 mission (at 1.6-m height); plus signs indicate the VL2 composite Sol (at 1.6-m height); and asterisks indicate the PF Sol (at 1.3-m height).

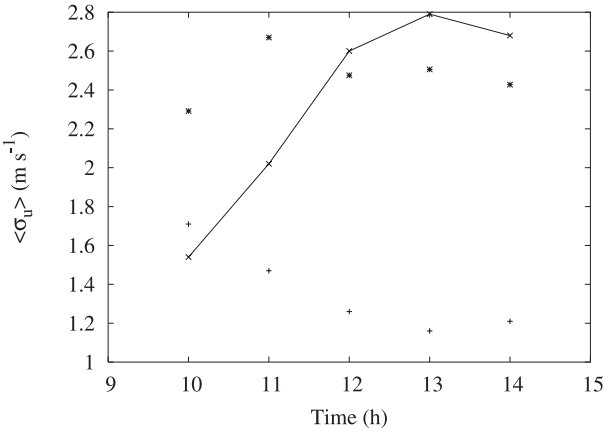

FIG. 8. Mean mixed layer horizontal wind speed standard deviation during the strongest convective hours for the three missions. Symbols are as in Fig. 7.

with the surface roughness (u_* dependence dominates L dependence) and there is virtually no dependence on the ground temperature scenarios, although the higher values take place under the *W* scenario because of the L dependence.

2) MIXED LAYER

We have derived the mean horizontal velocity standard deviation $\langle\sigma_u\rangle$ using Eq. (4). The mean value of this magnitude is expected to be representative of the whole MML because σ_u/w_* shows very little variation on z/z_i in the Earth. Values of $\langle\sigma_u\rangle$ (shown in Fig. 8) lie between 1.2 and 2.8 m s^{-1}, slightly higher than those calculated by Sorbjan (2007a) for a generic run. As this parameter depends only on w_*, its value does not depend on the inclusion of the molecular sublayer, the different surface roughness values, or the ground temperature scenarios, as is the case for w_*.

To obtain $\langle\sigma_w\rangle$, we have employed two different approaches. On the one hand, mixed layer similarity has been used via Eq. (3), which, after having been integrated across the mixed layer, results in $\langle\sigma_w\rangle \simeq 0.55w_*$. It is obvious that the use of the last relation demands that we question the reliability of the average value. That is, does σ_w vary strongly across the mixed layer with regard to the mean value $\langle\sigma_w\rangle$? What we have found is that the order of magnitude of this variable primarily remains unchanged across the MML, whereby the reliability of this result becomes stronger. To prove it, σ_w maximum values for all z have been calculated using Eq. (3) with the extreme calculated values of w_* and z_i. Results have always been the same order of magnitude. The second approach, Eq. (7), involves using the surface layer input. The results extracted from applying both techniques are shown in Fig. 9, where it can be seen that the values obtained are quite similar and lie within the range (1.2, 2.8) m s^{-1}. They also match those obtained in Rafkin et al. (2001) and Sorbjan (2007a), both of whom use LES for generic runs. Finally, the mean vertical wind speed standard deviation depends neither on the inclusion of the molecular sublayer nor on the surface roughness or the T_g scenarios.

As for $\langle\sigma_w\rangle$, we have determined the mean temperature standard deviation $\langle\sigma_\theta\rangle$ by two procedures. The first involves mixed layer similarity [see Eq. (5)], whereas surface layer parameters are involved in the second [see Eq. (8)]. The mean temperature standard deviation is also expected to represent typical MML values because extreme values for all z of σ_θ do not exceed the order of magnitude of $\langle\sigma_\theta\rangle$. In Fig. 10, values of this parameter are displayed, mainly ranging from 0.2 to 0.5 K. These values are similar to the ones shown in Sorbjan (2007a) for a generic run. Turning to the dependence relations, $\langle\sigma_\theta\rangle$ values decrease with the inclusion of the molecular sublayer, given that T_* also decreases and u_* and w_* remain unchanged. On the other hand, there exists virtually no variation regarding the surface roughness. Finally, maximum values are found under the *W* scenario because of the T_* dependence. However, around 18% variation is found between the *W* and the *C* scenarios.

c. *Turbulent viscous dissipation rate and eddy transfer coefficients*

1) SURFACE LAYER

We have derived these magnitudes following the methodology explained in Martinez et al. (2009). Representative values for the three sites during the strongest

Unauthenticated | Downloaded 12/10/24 11:25 AM UTC

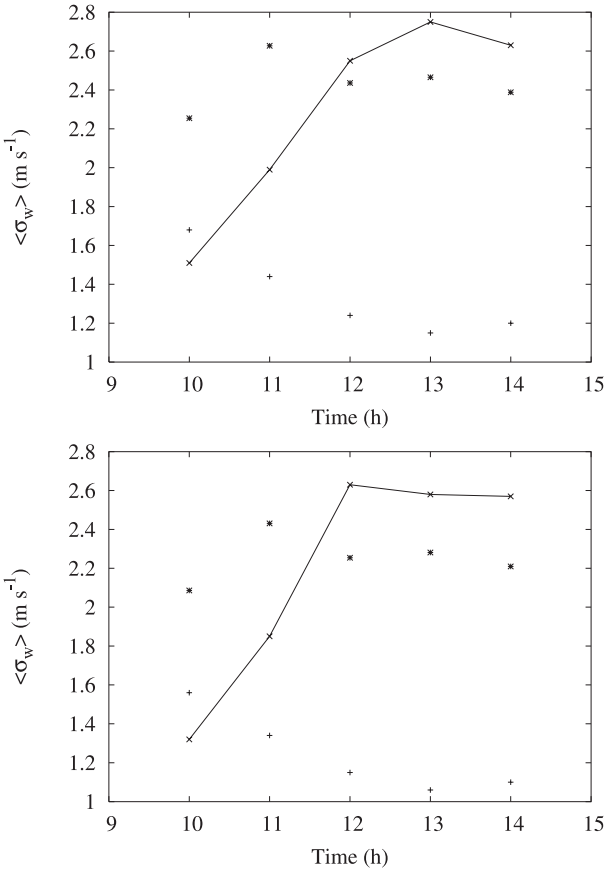

FIG. 9. Mean mixed layer vertical wind speed standard deviation during the strongest convective hours for the three missions corresponding to (top) Eq. (7) and (bottom) Eq. (3). Symbols are as in Fig. 7.

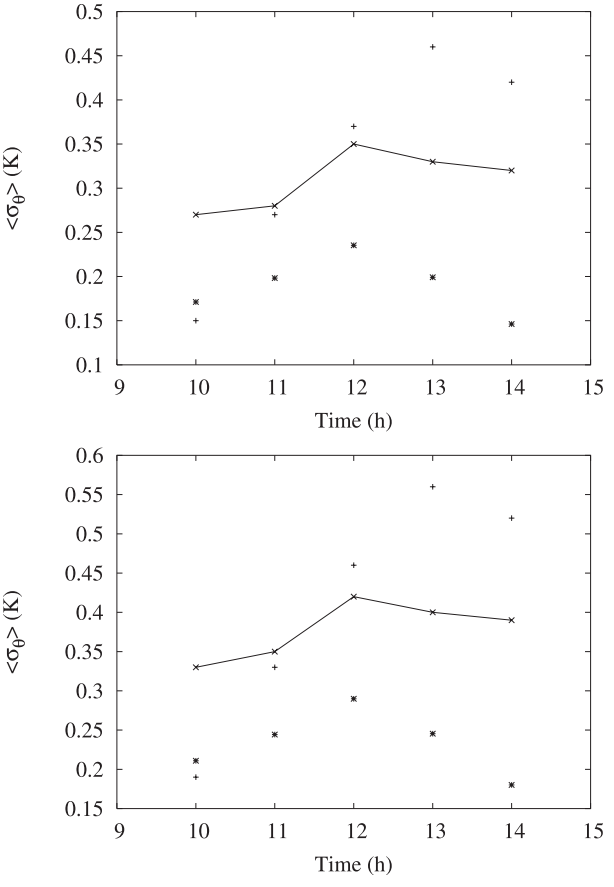

FIG. 10. Mean mixed layer temperature standard deviation during the strongest convective hours for the three missions corresponding to (top) Eq. (8) and (bottom) Eq. (5). Symbols are as in Fig. 7.

convective hours can be seen in Table 5. Values corresponding to the eddy transfer coefficients are around 0.3–0.4 m s^{-2}, the coefficient for heat transport being slightly higher. In the case of ϵ^z, its maximum values are around 0.1 m^2 s^{-3}. Eddy transfer coefficients and the turbulent viscous dissipation rate are slightly higher when calculated without the molecular sublayer (around 6% for both magnitudes). They both grow with the surface roughness and remain almost unchanged under the three T_g scenarios, although the *W* scenario shows slightly higher values for both magnitudes.

2) MIXED LAYER

We have determined the mean mixed layer turbulent viscous dissipation rate $\langle\epsilon\rangle$ from Eq. (6). Its evolution is shown in Fig. 11, where it can be observed that its values are on the order of 0.005 m^2 s^{-3}. This is in accordance with the fact that dissipation balances the buoyancy term of the turbulent kinetic energy equation across the mixed layer, which has been supposed to derive Eqs. (7) and (8). According to Tennekes (1970), $\langle\overline{w'\theta'}\rangle \simeq 0.2\langle\sigma_w\rangle\langle\sigma_\theta\rangle$ under strong convection. By substituting the values $g = 3.7$ m s^{-2}, $T_g = 270$ K, and the mean values that we have obtained for the standard deviations, we obtain a value on the order of 0.005^2 s^{-3} for the factor $(g/T_g)\langle\overline{w'\theta'}\rangle$; that is, it matches the value we have estimated for $\langle\epsilon\rangle$. Regarding the dependence relations, $\langle\epsilon\rangle$ decreases with the inclusion of the molecular

TABLE 5. Eddy diffusivity coefficients for momentum k_m and heat k_h, as well as the turbulent viscous dissipation rate ϵ, during the convective hours for the three missions. These magnitudes have been calculated at around 1.6 m for VK and 1.3 m for PF. The values shown correspond to the average performed on a composite Sol formed by Sols 27, 28, and 35 for the VL1 site and Sols 20 and 25 for the VL2 site.

	VL1	VL2	PF
k_m (m s^{-2})	0.4	0.2	0.25
k_h (m s^{-2})	0.45	0.35	0.30
ϵ (m^2 s^{-3})	0.20	0.02	0.17

Unauthenticated | Downloaded 12/10/24 11:25 AM UTC

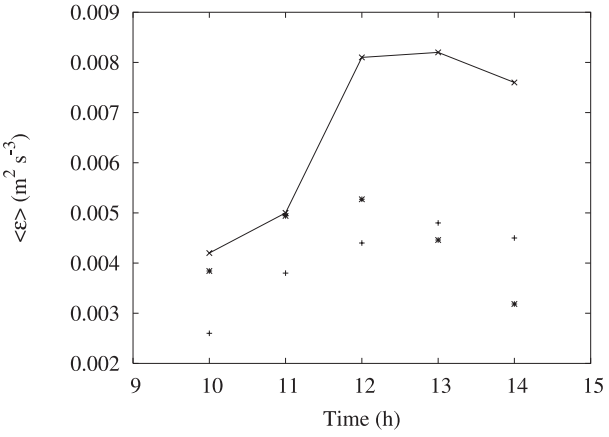

FIG. 11. As in Fig. 8, but for mean mixed layer turbulent viscous dissipation rate.

sublayer because z_i increases [see Eq. (6)]. Concerning the surface roughness, $\langle \epsilon \rangle$ grows with z_0, and its values under the *W* scenario are around 20% higher than *C* scenario results.

5. Discussion of the results

a. Comparison between MML and MLS magnitudes

Focusing on the results, Tables 6 and 7 can be used not only to compare the MPBL magnitudes to their terrestrial counterparts but also to compare the MSL magnitudes to their MML counterparts. Thus, we have found that turbulent temperature variations (standard deviations) become nearly as much 10 times greater in the first meters of the MSL than in the averaged MML. The same can be said about the scale temperatures. This is expected because similarity theory has been used, and hence $\theta_*/T_* \propto (-z_i/L)^{-1/3}$ is satisfied. The converse is true for turbulent vertical wind speed variations, given that $w_*/u_* \propto (-z_i/L)^{1/3}$, and therefore $\langle \sigma_w \rangle$ is expected to be higher than σ_w^z. More concretely and according to our results, it is about 5 times higher. In the case of horizontal wind speed standard deviation, we have obtained similar values both for the MSL and for the MML, in part because even in the MSL, σ_u^z scales with w_* instead of with u_*, as it does in the MML.

TABLE 6. Surface layer turbulent parameters on Mars and on Earth. Terrestrial values correspond to planetary boundary layers formed over flat and homogeneous terrain, and under no baroclinic disturbances. Martian results shown have been calculated for this paper.

Unstable surface layer	Mars	Earth
L	−17 m	Similar
u_*	~0.4 m s^{-1}	~0.3 m s^{-1}
$\lvert T_* \rvert$	~1 K	~0.15–0.4 K
		~0.27–0.88 K
ϵ^z	~0.16 m^2 s^{-3}	~0.01–0.02 m^2 s^{-3}, z = 4,32 m
		~0.001–0.01 m^2 s^{-3}, z = 18 m
σ_θ^z	~3 K	~0.18–0.32 K, z = 4 m
σ_u^z	~2 m s^{-1}	~1.4 m s^{-1}, z = 4 m
σ_w^z	~0.5 m s^{-1}	~0.4–0.6 m s^{-1}, z = 4 m
		~0.38–0.44 m s^{-1}, z = 4,32 m

TABLE 7. As in Table 6, but for the convective mixed layer.

Convective mixed layer	Mars	Earth
z_i	~6 km	~0.2–2 km
w_*	~4 m s^{-1}	~1.35–2.41 m s^{-1}
		~1−2 m s^{-1}
θ_*	~0.1 K	~0.05–0.1 K
		~0.03–0.07 K
$\langle \epsilon \rangle$	~0.005 m^2 s^{-3}	~0.001–0.005 m^2 s^{-3}
$\langle \sigma_\theta \rangle$	~0.3 K	~0.06–0.2 K
$\langle \sigma_u \rangle$	~2.4 m s^{-1}	~0.47–1.13 m s^{-1}
$\langle \sigma_w \rangle$	~2.4 m s^{-1}	~0.6–1.4 m s^{-1}

b. Sensitivity to surface roughness, to a molecular sublayer, and to ground temperature

Taking into account the fact that our results have been tested for different values of the surface roughness, under different ground temperature scenarios, and with and without the inclusion of a parameterized molecular sublayer, we summarize in Tables 8 and 9 their dependence on these ''external forcings.''

Starting with the temperature parameters (T_*, θ_*, and $\langle \sigma_\theta \rangle$), one may notice that they decrease if the inclusion of a molecular sublayer is carried out. This is something to be expected because, as was said before, the main consequence of including of the molecular sublayer is the surface heat flux decrease for a given air temperature and surface skin temperature difference. However, its inclusion has no effect on the wind parameters

TABLE 8. Dependencies on the molecular sublayer, on the surface roughness, and on the ground temperature scenarios for the calculated surface layer parameters under the strongest convective hours. Here, ↗ means to grow with, while ↘ to decrease with. The symbols ~↗ and ~↘ mean slightly increase with or slightly decrease with.

	Molecular sublayer	Surface roughness	T_g scenarios
$\lvert L \rvert$	~↗	↗	$\lvert L_C \rvert > \lvert L_{\mathrm{MPS}} \rvert > \lvert L_W \rvert$
u_*	—	↗	—
$\lvert T_* \rvert$	↘	—	$\lvert T_*^W \rvert > \lvert T_*^{\mathrm{MPS}} \rvert > \lvert T_*^C \rvert$
$k_{h,m}^z$	~↘	↗	$k_{h,m}^W \geq K_{h,m}^{\mathrm{MPS}} \geq k_{h,m}^C$
ϵ^z	~↘	↗	$\epsilon^W \geq \epsilon^{\mathrm{MPS}} \geq \epsilon^C$
σ_w^z	~↘	↗	$\sigma_w^W \geq \sigma_w^{\mathrm{MPS}} \geq \sigma_w^C$

Unauthenticated | Downloaded 12/10/24 11:25 AM UTC

TABLE 9. As in Table 8, but for the calculated mixed layer parameters.

	Molecular sublayer	Surface roughness	T_g scenarios
z_i	↗	↘	$z_i^C > z_i^{\mathrm{MPS}} > z_i^W$
w_*	—	—	—
θ_*	↘	~↗	$\theta_*^W > \theta_*^{\mathrm{MPS}} > \theta_*^C$
$\langle\epsilon\rangle$	↘	↗	$\langle\epsilon\rangle^W > \langle\epsilon\rangle^{\mathrm{MPS}} > \langle\epsilon\rangle^C$
$\langle\sigma_u\rangle$	—	—	—
$\langle\sigma_w\rangle$	—	—	—
$\langle\sigma_\theta\rangle$	↘	~↗	$\langle\sigma_\theta\rangle^W > \langle\sigma_\theta\rangle^{\mathrm{MPS}} > \langle\sigma_\theta\rangle^C$

(u_*, σ_w^z, w_*, $\langle\sigma_u\rangle$, and $\langle\sigma_w\rangle$) because the net effect on the transport of momentum is less noticeable. The behavior of the calculated parameters under the different T_g scenarios is the one that could be expected. That is, the higher the difference between the ground and the first meter (W scenario), the higher the value of these temperature parameters (T_*, θ_*, and $\langle\sigma_\theta\rangle$), whereas the wind parameters show less sensitivity. Concerning the surface roughness, MSL parameters show stronger dependence on it, whereas MML parameter dependence is virtually negligible in almost all cases.

c. *Comparison to the typical terrestrial planetary boundary layer*

Let us turn now to compare the values of the parameters obtained from the two planets. The Earth values shown correspond to planetary boundary layers formed over flat and homogeneous terrain, and under no baroclinic disturbances.

We start the comparison for the mixed layer on Mars and on Earth (see Table 7). The papers used to get the terrestrial results are Stull (1988) for z_i; Lenschow et al. (1980) for w_*, θ_*, and $\langle\sigma_w\rangle$; Kaimal et al. (1976) for w_*, θ_*, $\langle\epsilon\rangle$, and $\langle\sigma_\theta\rangle$; and André et al. (1978) for $\langle\sigma_u\rangle$. Notice that almost all Martian values are higher than their terrestrial counterparts. Specifically, we have found that the convective velocity scale and mean wind speed standard deviations are between 2 and 4 times higher in the MML, and hence so is the mean turbulent kinetic energy. This was also pointed out in Rafkin et al. (2001) using LES. That paper also mentioned that turbulence was not isotropic, as a result of vertical velocity variance being higher than the horizontal one. However, at least using mean values, similar values for both horizontal and vertical wind speed variances have been estimated in our calculations. The mean temperature standard deviation and convective temperature scale have also been found to be higher on Mars. This is expected because $\langle\sigma_\theta\rangle$ is proportional to θ_*, which in turn is also proportional to T_*, which is quite high because of the strong temperature gradients that prevail in the first meters on Mars. The mixed layer height, as has been already remarked by other authors, is much higher on Mars because of the much more vigorous existing convection.

We have carried out the same comparison with the characterizing surface layer parameters under unstable conditions (see Table 6). The articles consulted for the terrestrial results are Champagne et al. (1977) for ϵ^z, σ_θ^z, and σ_w^z; Kaimal et al. (1976) for T_* and σ_w^z; Lenschow et al. (1980) for T_*; and Panofsky et al. (1977) for σ_u^z. Remember that the Martian parameters have been estimated at 1.3 m for the PF and 1.6 m for the VL cases, whereas for the terrestrial case the height is indicated in Table 6. Typical values of L, u_*, σ_u^z, and σ_w^z agree on both planets. On the other hand, T_* and σ_θ^z are around one order of magnitude higher on Mars. The reason that lies behind these results can be explained as the sum of the following circumstances: (i) the net radiation that reaches the Martian soil is similar to that reaching the terrestrial soil, (ii) sensible and latent fluxes are much lower on Mars (low atmospheric density and virtual absence of water vapor), (iii) the thermal inertia shows lower values on Mars, and (iv) the air atmospheric density is very low. This all implies much higher temperature gradients at the first meters and consequently higher values of T_* and σ_θ^z.

6. Summary and conclusions

In this paper, the Martian planetary boundary has been thoroughly investigated. To do this, the main two layers that form the convective boundary layer have been characterized by determining several parameters. Values for the mixed layer height z_i, convective velocity scale w_*, convective temperature scale T_*, mean temperature standard deviation $\langle\sigma_\theta\rangle$, mean wind speed standard deviations $\langle\sigma_u\rangle$ and $\langle\sigma_w\rangle$, and mean turbulent viscous dissipation rate $\langle\epsilon\rangle$, all calculated for the PF and VK sites, have been derived in this paper concerning the MML. In addition, to characterize the MSL in this work, we have provided parameters that include not only those already obtained, such as the Monin–Obukhov length L, friction velocity u_*, and scale temperature T_*, but also new ones, such as the vertical wind speed variance, turbulent viscous dissipation rate, and eddy transfer coefficients for heat and momentum. Together with our values obtained, throughout the paper we can find references to other Martian articles in which some of the above mentioned magnitudes have also been derived by other methods. Moreover, numerical values of the all terrestrial counterparts are included, as well as their references.

Unauthenticated | Downloaded 12/10/24 11:25 AM UTC

Data employed in this study are from VL and PF sites. Sols 27, 28, and 35 for the VL1 and Sols 20 and 25 for the VL2 were chosen, whereas for the PF site only Sol 25 was selected. Hourly in situ temperature and hourly in situ horizontal wind speed have been used from both missions, as well as simulated ground temperature. These all correspond to typical low midlatitude northern summertime conditions, and thus the results of this work are representative of such conditions.

MML parameters have been estimated using mixed layer similarity theory; the methodology used to derive the MSL results is explained in Martinez et al. (2009). For both the MML and the MSL, every magnitude we have derived in this paper has been calculated under the different simulated ground temperature scenarios, with and without the inclusion of a parameterized molecular sublayer, and for the three proposed surface roughness values (0.1, 1, and 10 cm). Tables 8 and 9 show the dependence between the results and the surface roughness, the molecular sublayer, and the ground temperature scenarios.

We now list the main conclusions of this work. Concerning the surface layer on both planets, we have derived similar values of L, u_*, σ_u^z, and σ_w^z, largely because horizontal wind speed on both planets in the first meters is quite similar. However, the scale temperature T_* and temperature standard deviation σ_θ^z are around one order of magnitude higher on Mars. With regard to the mixed layer, z_i values are much higher on Mars, mainly because of the much higher kinematic heat flux values prevailing on Mars. The mean standard deviations of horizontal $\langle \sigma_u \rangle$ and vertical $\langle \sigma_w \rangle$ wind speed are between 2 and 4 times higher on Mars, and hence so is the mean turbulent kinetic energy. Finally, the mean temperature standard deviation also becomes higher on Mars, given that it is proportional to θ_* and hence also proportional to T_*, the magnitude of which is one order higher on Mars.

It is worth mentioning the limitations of this work. As is explained in appendix C, radiative heating, although nonnegligible, has been neglected. This means that our results are not generic for the whole Martian planetary boundary layer, but are specific to the low midlatitude northern summertime sites at local times near noon (i.e. when convective heating dominates radiative heating the most). On the other hand, the set of similarity relationships used in this paper, although expected to be universal, has been calculated on Earth. Last, the ground temperature has not been measured in situ but is simulated, which constitutes another source of error. However, this kind of study is a first and necessary step toward a further understanding of the MPBL. In addition, we feel confident about the order of magnitude of the variables obtained in this work.

We believe that some actions should be carried out in future Martian missions not only to eliminate all these uncertainties but also to keep on improving our understanding of the MPBL (which remains an open question). In situ measurements of ground temperature (not measured yet) would be very useful because this is an important parameter driving the evolution of the MPBL. Simultaneous measurements at different heights of temperature, humidity, and vertical (never measured) and horizontal wind speed would allow direct estimation of heat, humidity, and momentum surface fluxes. Moreover, Earth surface layer similarity relationships could be tested. In doing all this, the sampling rate should be high enough to capture small time scale processes associated with the microscale (typically higher than 1 Hz), and the total sampling period should last no less than an hour. All these surface layer studies are within reach if we take into consideration the current technology available to us. Direct measurements of MML magnitudes will probably take longer to happen.

Acknowledgments. We thank the support from the Spanish Grants CGL2005-06966-C07-04, ESP2007-30839-E, and ESP2007-30487-E. We also thank Prof. Sävijärvi (University of Helsinki) for his advice on the use of his model and Prof. Murphy (New Mexico University) for providing us with wind data and helping us in the preparation of this paper. One of the authors thanks the partial support from the firm Arquimea S.L., and also M. Feito and C. Cegarra for helping us in the realization of the paper. Finally, we thank the referees for their useful advice to improve this article.

APPENDIX A

List of Symbols and Definitions

Monin–Obukhov length L: Scaling parameter used in the surface layer; thought to represent length above which buoyancy starts dominating shear.

Friction velocity u_*: Velocity scale in the surface layer; a measure of the surface drag.

Scale temperature T_*: Temperature scale in the surface layer. Typical eddy temperature fluctuations in the surface layer.

Turbulent viscous dissipation rate ϵ^z: The conversion of turbulent kinetic energy into heat; calculated at the measuring height.

Unauthenticated | Downloaded 12/10/24 11:25 AM UTC

Potential temperature variance σ_θ^z: Calculated at the measuring height and averaged over intervals of 1 h.

Horizontal wind speed variance σ_u^z: Calculated at the measuring height and averaged over intervals of 1 h.

Vertical wind speed variance σ_w^z: Simulated at the measuring height.

Mixed layer height z: Often defined as the most negative heat flux level.

Convective scaling velocity w_*: The scaling velocity for the mixed layer; its value matches the magnitude of the vertical velocity fluctuations in thermals.

Convective temperature scale θ_*: The scaling temperature for the mixed layer; its values approximately represent how much warmer thermals are than the environment.

Mean mixed layer turbulent viscous dissipation rate $\langle \epsilon \rangle$: Conversion of turbulent kinetic energy into heat; averaged over the whole mixed layer.

Mean mixed layer potential temperature variance $\langle \sigma_\theta \rangle$: Corresponds to the average over the whole mixed layer.

Mean mixed layer horizontal wind speed variance $\langle \sigma_u \rangle$: Corresponds to the average over the whole mixed layer.

Mean mixed layer vertical wind speed variance $\langle \sigma_w \rangle$: Corresponds to the average over the whole mixed layer.

APPENDIX B

Simulated Ground Temperature

We have used a version of the 1D model presented in Savijärvi et al. (2004) to simulate the ground temperature during the selected Sols at the three different sites. Because the model needs some external parameters to be run, we have taken advantage of articles in which those external parameters that most influence simulated T_g (thermal inertia, albedo, dust optical depth, surface emissivity, etc.) have been estimated, as in Christensen et al. (2001) and Putzig et al. (2005), or have simply been imposed, as in existing articles involving the Sävijärvi 1D model and Haberle et al. (1993). Within the found range of values of these external parameters, we have simulated three T_g scenarios: the MPS, the W, and the C scenarios (both expected and reliable extreme scenarios of ground temperature). For the MPS we require the best match between in situ and modeled air temperature, at 1.3 m for PF and 1.6 m for VK. The external parameters used to run the model for the MPS can be seen in Table 2. In creating the extreme scenarios, extreme values found for these parameters have been used to run the model, bearing in mind that T_g increases when surface emissivity decreases, T_g increases during daytime and decreases at night when thermal inertia or dust optical depth are decreased, and finally T_g increases during daytime and remains unaltered at night when albedo is decreased.

The superscripts *W*, *C*, and MPS have been added throughout the paper to any magnitude (for instance, L^W, L^{MPS}, and L^C) to denote that they have been calculated under the warmest, coldest, and most probable scenario, respectively.

APPENDIX C

On the Applicability of the Mixed Layer Similarity Theory to Mars

The main hypotheses that must be satisfied when applying mixed layer similarity theory are the following: (i) convection is the dominant heating mechanism throughout the mixed layer and (ii) surface stress effects become negligible through this layer. This is certainly so on Earth under fair weather conditions (André et al. 1978) because the heating rate due to the radiation divergence is negligible and the winds are light under these conditions. On Mars, however, special care must be taken. There is no uncertainty in neglecting the effects of the surface stress through the bulk of the MML because the winds were calm during the Sols under study (low midlatitude northern summertime). The problem arises with the radiative heating throughout the MML, which becomes nonnegligible due to the longwave radiative heating (CO_2 atmosphere) and the absorption of solar radiation by dust.

Two questions emerge immediately: How important is the radiative heating compared to the convective heating? And consequently, to what extent are our results reliable after having been calculated using a theory that neglects this radiative heating? Based on our results performed with a modified version of Savijärvi et al. (2004) and supported by Savijärvi (1991), Haberle et al. (1993), and Savijärvi (1999), the convective heating is between 2 and 3 times higher than the radiative one through the bulk of the MML, especially close to noon. In Sorbjan (2007a), this ratio can even reach a factor of 5 for early morning hours. The thin northern summertime atmosphere and the low atmospheric dust load existing during the Sols under study reduce the radiative heating strength, favoring the convective heating domain. Thus, convection still is the dominant mechanism, although radiative divergence cannot be ignored. All this leads us to keep using mixed layer similarity, while remembering the above discussion and the corresponding limitations (time of the year

Unauthenticated | Downloaded 12/10/24 11:25 AM UTC

and time of the day). Notice also that the results shown in the displayed figures range from 1000 to 1400 LT. Based on our results, convective heating becomes higher than the radiative one during these hours, and especially near noon, when it becomes about 3 times higher.

Once the first question has been answered, we move on to the second one. Sorbjan (2007a) found that magnitudes such as temperature and wind speed MML standard deviation do not change their order of magnitude after having introduced weak and strong radiative heating (see Figs. 7 and 10 of Sorbjan 2007a). With regard to the reliability of our results, we also expect them to be reliable concerning the order of magnitude, given that we have performed our research in the most favorable time of the year and of the day to avoid the issue of radiative heating.

REFERENCES

André, J. C., G. De Moor, P. Lacarrère, G. Therry, and R. du Vachat, 1978: Modeling the 24-hour evolution of the mean and turbulent structure of the planetary boundary layer. *J. Atmos. Sci.,* **35,** 1861–1883.

Arya, P., 2001: *Introduction to Micrometeorology*. Academic Press, 420 pp.

Blumsack, S., P. Gierasch, and W. Wessel, 1973: An analytical and numerical study of the Martian planetary boundary layer over slopes. *J. Atmos. Sci.,* **30,** 66–82.

Brutsaert, H., 1982: Exchange processes at the earth–atmosphere interface. *Engineering Meteorology,* E. Plate, Ed., Elsevier, 319–369.

Champagne, F., C. Friehe, J. LaRue, and J. Wyngaard, 1977: Flux measurements, flux estimation techniques, and fine-scale turbulence measurements in the unstable surface layer over land. *J. Atmos. Sci.,* **34,** 515–530.

Christensen, P., and Coauthors, 2001: Mars Global Surveyor Thermal Emission Spectrometer experiment: Investigation description and surface science results. *J. Geophys. Res.,* **106** (E10), 23 823–23 871.

Deardorff, J., 1970: Convective velocity and temperature scales for the unstable planetary boundary layer and for Rayleigh convection. *J. Atmos. Sci.,* **27,** 1211–1213.

Gierasch, P., and R. Goody, 1968: A study of the thermal and dynamical structure of the Martian lower atmosphere. *Planet. Space Sci.,* **16,** 615–646.

Haberle, R., H. Houben, R. Hertenstein, and T. Herdtle, 1993: A boundary-layer model for Mars: Comparison with Viking Lander and entry data. *J. Atmos. Sci.,* **50,** 1544–1559.

Hess, S., R. Henry, C. Leovy, J. Ryan, and J. Tillman, 1977: Meteorological results from the surface of Mars: Viking 1 and 2. *J. Geophys. Res.,* **82,** 4559–4574.

Kaimal, J. C., J. C. Wyngaard, D. A. Haugen, O. R. Coté, Y. Izumi, S. J. Caughey, and C. J. Readings, 1976: Turbulence structure in the convective boundary layer. *J. Atmos. Sci.,* **33,** 2152–2161.

Larsen, S., H. Jørgensen, L. Landberg, and J. Tillman, 2002: Aspects of the atmospheric surface layers on Mars and Earth. *Bound.-Layer Meteor.,* **105,** 451–470.

Lenschow, D., J. Wyngaard, and W. Pennell, 1980: Mean-field and second-moment budgets in a baroclinic, convective boundary layer. *J. Atmos. Sci.,* **37,** 1313–1326.

Määttänen, A., and H. Savijärvi, 2004: Sensitivity tests with a one-dimensional boundary-layer Mars model. *Bound.-Layer Meteor.,* **113,** 305–320.

Magalhaes, S., and P. Gierasch, 1982: A model of the Martian slope winds: Implications for eolian transport. *J. Geophys. Res.,* **87,** 9975–9984.

Martínez, G., F. Valero, and L. Vázquez, 2009: Characterization of the Martian surface layer. *J. Atmos. Sci.,* **66,** 187–198.

Michaels, T., and S. Rafkin, 2004: Large-eddy simulation of atmospheric convection on Mars. *Quart. J. Roy. Meteor. Soc.,* **130,** 1251–1274.

Odaka, M., 2001: A numerical simulation of Martian atmospheric convection with a two-dimensional anelastic model: A case of dust-free Mars. *Geophys. Res. Lett.,* **28,** 895–898.

Panofsky, H., H. Tennekes, D. Lenschow, and J. Wyngaard, 1977: The characteristics of turbulent velocity components in the surface layer under convective conditions. *Bound.-Layer Meteor.,* **11,** 355–361.

Putzig, N., M. Mellon, K. Kretke, and R. Arvidson, 2005: Global thermal inertia and surface properties of Mars from the MGS mapping mission. *Icarus,* **173,** 325–341.

Rafkin, S., R. Haberle, and T. Michaels, 2001: The Mars Regional Atmospheric Modeling System: Model description and selected simulations. *Icarus,* **151,** 228–256.

Savijärvi, H., 1991: A model study of the PBL structure on Mars and the earth. *Beitr. Phys. Atmos.,* **64,** 219–229.

——, 1995: Mars boundary layer modeling: Diurnal moisture cycle and soil properties at the Viking Lander 1 site. *Icarus,* **117,** 120–127.

——, 1999: A model study of the atmospheric boundary layer in the Mars Pathfinder lander conditions. *Quart. J. Roy. Meteor. Soc.,* **125,** 483–493.

——, and T. Siili, 1993: The Martian slope winds and the nocturnal PBL jet. *J. Atmos. Sci.,* **50,** 77–88.

——, A. Määttänen, J. Kauhanen, and A. Harri, 2004: Mars Pathfinder: New data and new model simulations. *Quart. J. Roy. Meteor. Soc.,* **130,** 669–683.

Schofield, J., and Coauthors, 1997: The Mars Pathfinder Atmospheric Structure Investigation/Meteorology (ASI/MET) Experiment. *Science,* **278,** 1752–1758.

Siili, T., R. Haberle, and J. Murphy, 1997: Sensitivity of Martian southern polar cap edge winds and surface stresses to dust optical thickness and to the large-scale sublimation flow. *Adv. Space Res.,* **19,** 1241–1244.

Sorbjan, Z., 2007a: Statistics of shallow convection on Mars based on large-eddy simulations. Part 1: Shearless conditions. *Bound.-Layer Meteor.,* **123,** 121–142.

——, 2007b: Statistics of shallow convection on Mars based on large-eddy simulations. Part 2: Effects of wind shear. *Bound.-Layer Meteor.,* **123,** 143–157.

Stull, R., 1988: *An Introduction to Boundary Layer Meteorology*. Springer, 670 pp.

Sutton, J., C. Leovy, and J. Tillman, 1978: Diurnal variations of the Martian surface layer meteorological parameters during the first 45 Sols at Two Viking Lander sites. *J. Atmos. Sci.,* **35,** 2346–2355.

Unauthenticated | Downloaded 12/10/24 11:25 AM UTC

Tennekes, H., 1970: Free convection in the turbulent Ekman layer of the atmosphere. *J. Atmos. Sci.,* **27,** 1027–1034.

Tillman, J., L. Landberg, and S. Larsen, 1994: The boundary layer of Mars: Fluxes, stability, turbulent spectra, and growth of the mixed layer. *J. Atmos. Sci.,* **51,** 1709–1727.

Toigo, A., and M. Richardson, 2002: A mesoscale model for the Martian atmosphere. *J. Geophys. Res.,* **107,** 5049, doi:10.1029/2000JE001489.

——, ——, S. Ewald, and P. Gierasch, 2003: Numerical simulation of Martian dust devils. *J. Geophys. Res.,* **108,** 5047, doi:10.1029/2002JE002002.

Ye, Z., M. Segal, and R. Pielke, 1990: A comparative study of daytime thermally induced upslope flow on Mars and Earth. *J. Atmos. Sci.,* **47,** 612–628.

Zeng, X., and R. Dickinson, 1998: Effect of surface sublayer on surface skin temperature and fluxes. *J. Climate,* **11,** 537–550.

Unauthenticated | Downloaded 12/10/24 11:25 AM UTC